Structural, optoelectronic, thermal and transport properties of hybrid perovskite ($EAGeCl_3$) material

A. Dubey[a], K. Mishra[b], R. Srivastava[c], A. Kumari[d], P. K. Jangra[e], T. K. Joshi[f], B. L. Choudhary[a], A. S. Verma[g,h,*]

[a]*Department of Physical Sciences, Banasthali Vidyapith, Rajasthan 304022, India*
[b]*Department of Mathematics, Noida Institute of Engineering and Technology (NIET), Greater Noida, 201306, India*
[c]*Department of Electronics and Communication Engineering, KIET Group of Institutions, Ghaziabad 201206, India*
[d]*Department of Physics, S. V. College, Raja Mahendra Pratap Singh State University, Aligarh, 202140, India*
[e]*Department of Chemistry, Government College for Women, Badhra, Charkhi Dadri, 127308, India*
[f]*Department of Physics, Swami Vivekanand Govt. P. G. College, Neemuch, Madhya Pradesh 458441 (India)*
[g]*Division of Research and Innovation, School of Applied and Life Sciences, Uttaranchal University, Dehradun, 248007, India*
[h]*University Centre for Research & Development, Department of Physics, Chandigarh University, Mohali, Punjab, 140413, India*

Hybrid halide perovskites are emerging as an encouraging option for the fabrication of solar systems. Ethyl-ammonium-based hybrid halide perovskites offer amazing qualities such as reduced bandgap, increased structure stability, and less toxicity. Properties like structural; electrical; optical; and thermoelectric of the material ethyl ammonium germanium chloride are calculated using density functional theory (DFT) simulation code WIEN2K and calculated the optimized structure; density of states; and band structure of $EAGeCl_3$ using exchange-correlation potential KTB-mBJ, establishing it as a direct bandgap semiconductor. Several optical properties such as dielectric function; absorption coefficient; and refractive index over a photon energy spectrum over the range of 0 to 7 eV have also been calculated. In addition, transport coefficients also calculated dependent on concentration of charge carriers, the chemical potential, and temperature at which the material is operating. The findings emphasize the extraordinary properties of $EAGeCl_3$, which has a high ability to absorb electromagnetic radiation, such as light, with a high efficiency, superior compound's ability to generate an electric potential in response to temperature, among additional benefits. These discoveries confirm its suitability as an affordable material for use in photovoltaic devices, contributing to the resolution of environmental concerns.

(Received March 20, 2024; Accepted June 10, 2024)

Keywords: Ethylammonium organometallic perovskites, Bandgap, Seebeck coefficient, Electrical conductivity, Thermal conductivity

1. Introduction

Photovoltaic systems are utilized for capturing solar energy and transforming it into electrical power. To achieve effective conversion of solar energy, PV absorber materials with distinct physical properties are necessary. These attributes encompass an appropriate direct bandgap within the visible spectrum, high solar energy absorption, highly mobilized carrier and superior efficiency in converting solar energy to electricity [1-4]. Furthermore, these materials must exhibit stability in a humid environment under elevated ambient temperatures [5]. In

* Corresponding author: ajay_phy@rediffmail.com
https://doi.org/10.15251/JOR.2024.203.381

addition, top-quality thermoelectric materials must have high current carrying capacity, a significant Seebeck coefficient, and low thermal conductivity [6-9]. Recently, a hybrid halide perovskite absorber with a lead-based composition emerged with physical promising characteristics for applications. These materials are denoted by the general formula $APbX_3$, with a representing $CH_3NH_3^+$ cation and X^- signifying a halide anion [10-12]. Lead-based halide perovskites offer a cost-effective and efficient solution for solar power conversion, with a conversion rate ranging from 15-22% [13-17]. However, their practical use in commercial settings is impeded by the presence of toxic lead and their susceptibility to high temperatures, strong sunlight, and humidity [18-21]. To address such drawbacks, the researchers are diligently investing alternative options that are free of lead, non-toxic and environmentally friendly [22]. In this study, the main aim is to find a suitable lead-free perovskite PV material by replacing the methyl-ammonium ion ($CH_3NH_3^+$) with the ethyl-ammonium ion ($CH_3CH_2NH_3^+$) and the lead ion (Pb^{2+}) with the Germanium ion (Ge^{2+}) in the lead-based PV material known as $CH_3NH_3PbCl_3$.We have anticipated that the resulting material, $CH_3CH_2NH_3GeCl_3$ or $EAGeCl_3$, would possess all the desired properties necessary for efficient PV applications.

Liu et al. [23] have shown that combining EA and MA cations results in $EAPbI_3$, which shows potential as a reliable candidate for photovoltaic applications. Zhang et al. [24] have experimentally demonstrated an impressive 18% power conversion efficiency of $EAPbI_3$. Joshi et al [25] found that $EAPbI_3$ has a direct band gap (1.55 eV) and an absorption coefficient of 2×10^4 per cm, indicating its potential for use in solar cells. They also discovered that EASnI3 is characterized by the direct bandgap which equals to 1.17 eV, a high Seebeck coefficient, and large figure of merit [26]. It was indicated by Arkan et al [27] that $EAGeCl_3$ may be employed as an additive to improve charge transfer at the interface between different layers in perovskite solar cells due to its suitable physicochemical and photovoltaic properties. Furthermore, according to Joshi et al [28], $EAGeI_3$ demonstrates n-type semiconductor behavior with a direct bandgap of 1.30 eV and ZT>0.9 at doping level $\sim10^{18}$ cm^{-3}, thus showing promise for thermoelectric applications.

By considering these studies and aiming at reducing lead content in perovskite materials, we have chosen $EAGeCl_3$ compound for investigation purposes. We involves performing DFT calculations using the WIEN2K package so as to comprehend various structural, electronic, optical as well as thermo-physical aspects associated with this material type.

2. Methodology

DFT is the present-day and generally accepted method for performing ab initio calculations that determine the basic properties of materials at their ground state [29]. DFT could be used to determine the geometry of a material, understand its structure completely with explanation and describe bonding between ions in the system. The research utilizes the approach of full potential linearized augmented wave (FP-LAPW) within DFT, as utilizing the WIEN2K code for computational analysis [30]. This code has different calculations such as dispersion curves and density of states, which can be performed using different approximations, including local density approximation (LDA) [31] and generalized gradient approximation (GGA) [32]. However, these approximations tend to underestimate the bandgap of rock salt structures.

While the hybrid function [33] and GW method [34] have been employed as effective approximations for exchange-correlation potential, their significant computational expenses prompt us to explore alternative approximations. To calculate the position of atoms, lattice constant (a), bulk modulus (B), minimum energy (E_0), and the first derivative of Bulk modulus (B') an optimized structure is used. This optimization process continued till then the residual force on atomic sites was reduced and lower than, 10^{-3} Ry $Bohr^{-1}$. The energy required to separate the core and valance states was determined to be -0.6Ry. This energy also referred to as the cutoff energy [35]. The basis set within each muffin-tin sphere (MTS) is parted into two subsets first is core and the second valance subsets [36]. The first state is assumed to be handled in spherical region of the potential and is assumed exhibit particularly symmetric charge density, entirely

confined within the MTS. In our current study, we established muffin-tin radii (RMT) for H 0.6, for N 1.25, for C 1.20, for Cl 2.37 and Ge 2.50 respectively.

There are lots of band gap underestimation issues observed with LDA, PBE, WC, and PBE-Sol [37] approximations. To defeat this challenge, Koller, Tran, and Blaha introduced the KTB-mBJ [38] potential. This potential is propose a computational.ly simpler exchange that significantly enhances the energy gap value for multiple semiconductor materials. This approximation can be referred to as:

$$V_x^{TB-mBJ}(r) = cv_x^{BR}(r) + (3c-2)\frac{1}{\pi}\left[\frac{5}{12}\right]^{\frac{1}{2}}\left[\frac{2t(r)}{\rho(r)}\right]^{\frac{1}{2}} \quad (1)$$

where, $t(r)$ and $v_x^{BR}(r)$ are the Kohn-Sham kinetic energy density [39] and the Becke-Roussel exchange potential [40], $\rho(r)$ and c are the electron density and; free parameters. Electronic characteristics are assessed employing 700k points, whereas optical parameters are computed using 10000k points across the irreducible Brillouin zone. Thermodynamic properties are derived utilizing 10000k points with the Boltztrap code, and for the thermal properties, the Gibbs2 package is employed.

3. Results and discussion

3.1. Structural properties

The cubic structural arrangement of $CH_3CH_2NH_3GeCl_3$ is presented in figure 1.

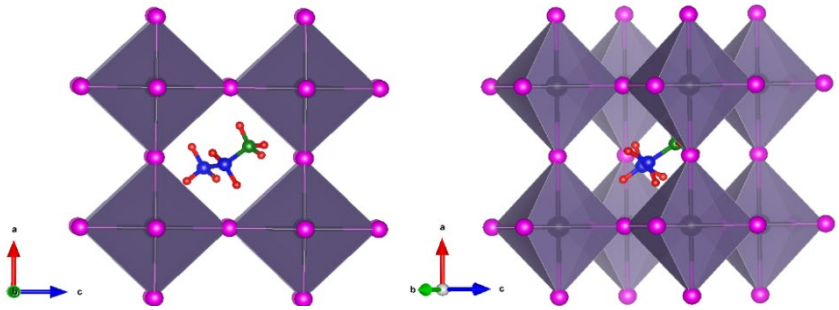

Fig. 1. Optimized Crystal structure of $C_2H_5NH_3GeCl_3$ material. The red, blue and green are H, N and C atoms respectively. Within the octahedral structure of Ge cation, there are Cl anions are located at the corner.

In this configuration two cations are present ($CH_3NH_3^+$, Ge^{2+}). They show significant size disparity as they establish bonds with the anion Cl^-. The Ge^{2+} cation is positioned within coordination, encircled by an octahedron composed of Cl atoms. Simultaneously, the $CH_3CH_2NH_3^+$ cation is situated in the interstitial site between the $GeCl_3$ octahedron. To comprehend the material's response to temperature and pressure, it is essential to ascertain the material's structural parameters. Employing the Birch-Murnaghan's equation of state; we conduct optimization of the volume calculation for the lattice constant [41]. The Birch-Murnaghan's equation is represented as [42]:

$$E(V) = E_0 + \frac{9V_0B_0}{16}\left\{\left[\left(\frac{V_0}{V}\right)^{2/3} - 1\right]B_0' + \left[\left(\frac{V_0}{V}\right)^{2/3} - 1\right]^2 \times \left[6 - 4\left(\frac{V_0}{V}\right)^{2/3}\right]\right\} \quad (2)$$

Figure 2 illustrates the curve fitting of energy (E) vs per unit cell volume (V), while Table 1 provides the optimized parameter of $EAGeCl_3$. Notably, as the size of halide ion increases from Chlorine to Iodine, there is a corresponding increase in the lattice constant [43]. This theoretical

fact fitted well with the Joshi et al [28] report, the value of a lattice constant of 6.387 Å for $EAGeI_3$, confirming the structure stability of the $EAGeCl_3$ compound.

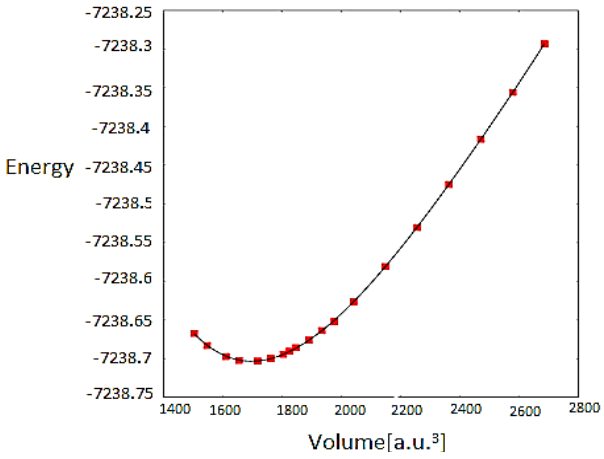

Fig. 2. Optimization curve of per unit cell total energy Vs volume.

Table 1. Optimized parameters of $EAGeCl_3$.

Material.	V_0 (Å^3)	a (Å)	B (GPa)	B'
$CH_3CH_2NH_3GeCl_3$	1694.4829	6.308	42.1877	3.45

3.2 Electronic properties

In our ongoing investigation, we initiated the exploration of the band structure of the specified compound as a fundamental starting point. The electronic band structure of the material, along with the electron arrangement within those bands, plays a crucial role in determining its applications. In Figure 3, the valance electronic charge density shows the ion behavior of Ge-Cl bond.

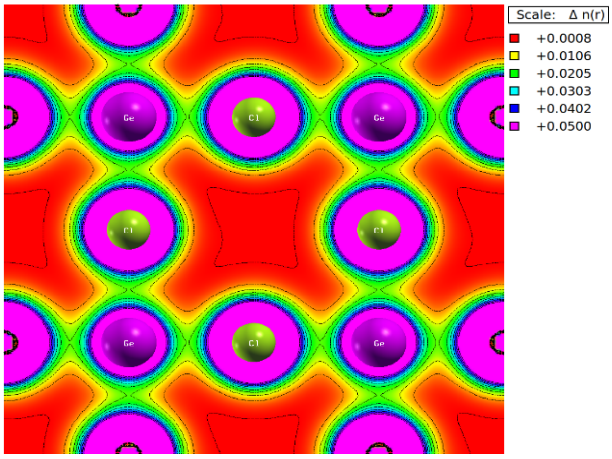

Fig. 3. Electronic charge density plot $EAGeCl_3$ cubic perovskite.

The electrical properties of $EAGeCl_3$ are influenced by the bond between Ge and Cl, the angle of the bond in Cl-Ge-Cl. The ionic nature of this Ge-Cl bond is revealed through circular contours of the density of electrons in valance states which is centered on Cl and Ge. However,

analysis of the outermost contours in the figure indicates a sharing of valance electrons between Cl and Ge, suggesting a covalent character in the Ge-Cl bond. The effective mass of the charge significantly influences the investigation of the PCEs of PV devices. The effective mass is increased as the mobility of charge carriers decreases. For determining the effective mass (m*) of charge carriers, a parabolic fit is applied to minima or maxima of both the conduction band (CB) and valance band (VB) at a symmetry point R within the band-edge. These fitting of the parabola are done by the given equation:

$$m^* = \hbar^2 \left[\frac{\partial^2 E(k)}{\partial k^2}\right]^{-1}$$

The above equation contains the wave vector (k) and; the E(k) is the energy-eigen value at the symmetry point R.

Table 2. Effective mass of $EAGeCl_3$.

Material	m_e^*	m_h^*
$EAGeCl_3$	$0.76m_e$	$0.61m_e$

The content presented in graph 4 displays the band structure and density of states. It shows how energy (E) is related to the wave vector (k) within the FBZ, which is a range of wave vectors representing electron states in a crystalline material in the case of $EAGeCl_3$. The inherent characteristics or behavior of $EAGeCl_3$ as a semiconductor material without any external influences such as doping the band gap is not occupied by any electronic states.

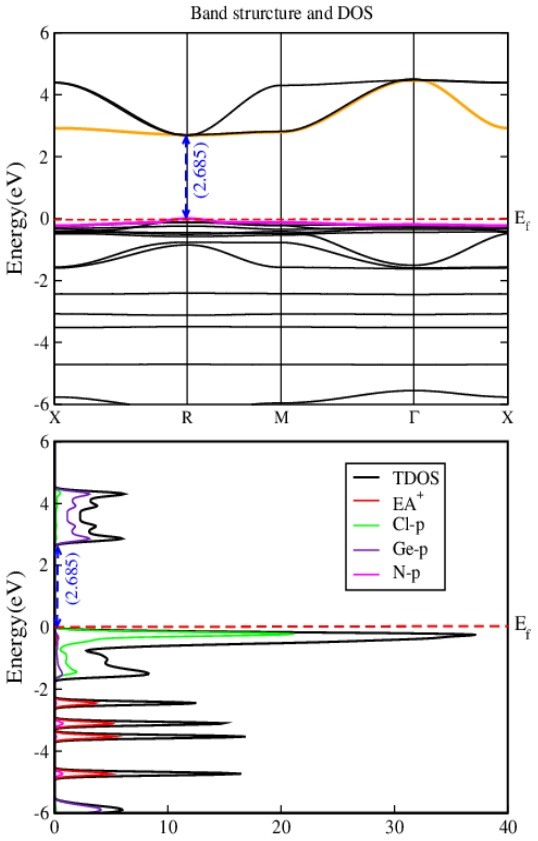

Fig. 4. The band structure and the Density of states plot of $EAGeCl_3$.

Furthermore, maximum energy level in the valance band and the minimum energy level in conduction band are positioned at the symmetry point R-position. Because both VBM and CBM are presented at the same symmetry, the band gap between them direct rather than indirect and the value of this direct band gap is approximately 2.685 eV. The observed energy band gap arises from the evolution of the CB and; VB through the intersecting of; Ge-4p; Ge-4s; and Cl-3p orbitals. The observed reduction in the band gap as the size of halide ions (from chloride, Cl, to iodide, I) increases, there is a corresponding decrease in the band gap value. This relationship is likely due to the change in the crystal lattice structure and the atomic size of the halide ions, which influences the electronic structure of the material [44]. Joshi et al [28] stated the band gap of 1.30 eV $EAGeI_3$.This result is smaller than the bandgap for $EAGeCl_3$ and verifies the theoretical variation in the bandgap.

For a complete examination of the band structure of $EAGeCl_3$, the TDOS and PDOS are calculated. This study is important to show the semiconductor behavior of the material. The energy states from -6 to 0 eV are occupied and reside lower side of the Fermi level and another range of energy states, from 0 to 6 eV above the Fermi level, where no electrons are present. To get the particular ion behavior partial density of states is studied for EA^+; Sn; and; Cl atoms. The green color peak at 0 to -2 eV below the Fermi level is due to the electrons from Cl-3p states. The presence of a red color peak in the range of -3 eV to -4 eV signifies the modest benefaction of the EA^+ ion. Conversely, the purple peak situated above the Fermi-energy level (3-5 eV) is ascribed to the involvement of the unoccupied Ge-4p states. Within the energy span from 0 to 2.685 eV, no permissible states are observed; instead, a forbidden band gap is present.

3.3. Optical properties

The material's dielectric function in equation (3), is directly associated to optical properties. The absorption of energy within the visible region significantly influences the control or adjustment of various optical characteristics of a material, such as its transparency, color, and refractive index, regardless of its composition or structure. This is typically achieved by determining the band gap and absorption coefficient of the materials.

$$\varepsilon(\omega) = \varepsilon_1(\omega) \pm \varepsilon_2(\omega) \tag{3}$$

Here $\varepsilon_1(\omega)$ represents the real component of the dielectric function; related to the ability to store energy when exposed to an electric field and redistribution of charge within the material when an external electric field is applied on the material. On the other hand, $\varepsilon_2(\omega)$ denotes imaginary component of dielectric function; responsible for reducing the strength of the wave and the loss of energy as the wave propagates through the material, in the form of heat. In figure 5(A), a plot of $\varepsilon_1(\omega)$ vs photon energy is presented.

The findings suggest that the real part of the dielectric constants for $EAGeCl_3$ is increases from the visible region to the infrared. The electronic component of the static dielectric constant$\varepsilon_1(0)$ is readily observed in the low energy limit of the dielectric function $\varepsilon_1(\omega)$ and is found to be 2.59. At 2.97 eV, $EAGeCl_3$ reaches its maximum $\varepsilon_1(\omega)$ value of 5.16, marking the first intra-band transition in the BZ. Figure 5(B) illustrates the optical properties of the imaginary part $\varepsilon_2(\omega)$ of the dielectric function with respect to photon energy. The graphs depict the material's maximum absorption behavior. A closer examination of the TDOS and PDOS spectrum for $EAGeCl_3$ suggests a direct transition between the filled VB states of Cl-3p and Ge-4s, and the unoccupied CB states of Ge-4p and Cl-3p. The other peak represents the movement of electrons in inter-band transitions between the VB and CB. The refractive index is a crucial factor in optics by providing information of light behavior in different materials. Light travels from different medium, speed of light changes, which results the change in the refractive index. Graph 5(C) illustrates the change in refractive index for photon energy. For $EAGeCl_3$, the constant refractive index at zero energy value $n(0)$ is determined to be 1.61. The highest refractive index is 2.32 at 3.03 eV in the visible region. The extinction coefficient is a crucial factor that indicates a material's ability to absorb light at a specific frequency. It represents the imaginary component of the $n(\omega)$. It reflects the capability of an electromagnetic wave to propagate from a medium. In figure 5(D), the extinction coefficient varies with photon energy, peaking at 3.74eV with a value of 1.44.

Figure 6(A) illustrates the absorption coefficient $\alpha(\omega)$ of $EAGeCl_3$. The absorption coefficient reflects the power of material to soak up energy. In graph, there is significant increase observed when the value exceeds zero. The most significant increment is shown when the photon energy passes the band gap (2.685 eV). When the energy of the photon is 3.82 eV, the d value reaches its peak at 55.14×10^4 cm^{-1}. In the visible spectrum from red to violet, this coefficient show a linear increase from 0.2×10^4 cm^{-1} and reaching 25.13×10^4 cm^{-1}. Coefficient values greater than 10^4 cm^{-1} indicate high chance of direct transitions.

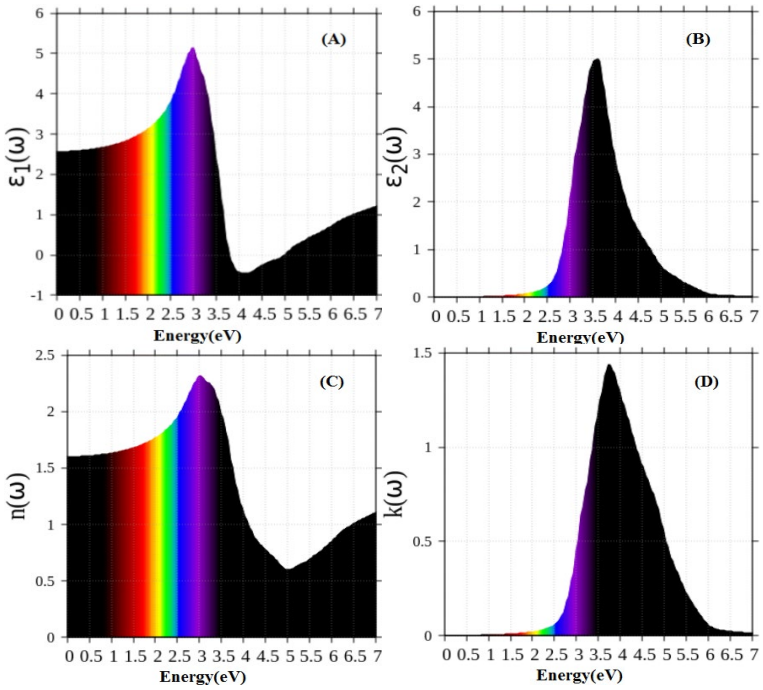

Fig. 5. (a) Real part of dielectric function, (b) Imaginary part of dielectric function, (c) Refractive index, and (d) Extinction coefficient.

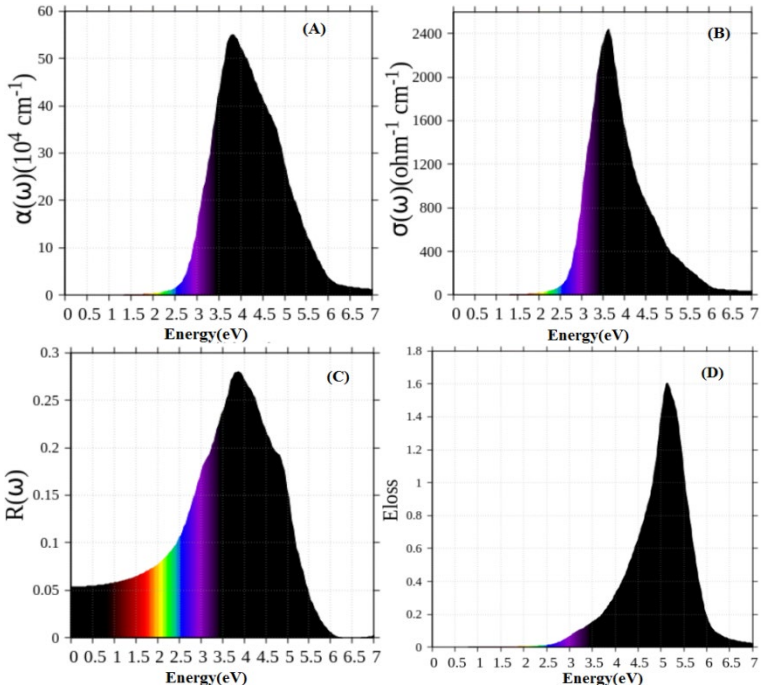

Fig. 6. (a) Optical absorption coefficient, (b) Optical conductivity, (c) Reflectivity, and (d) Electronic energy-loss function.

Therefore, we can conclude that $EAGeCl_3$ exhibits absorption coefficients suitable for use in photovoltaic technologies. In our specific context, this phenomenon occurs from the direct transition from the filled Cl-3p and Ge-4s VB states to the vacate Ge-4p to Cl-3p CB states. The optical conductivity $\sigma(\omega)$ is graphed in figure 6(B). $\sigma(\omega)$ starts to increase the photon energy passes the bandgap (2.685 eV). At 3.57 eV it reaches its maximum value of 0.24×10^4 $\Omega^{-1}cm^{-1}$. The optical reflectivity properties of the $EAGeCl_3$ material are graphically depicted in figure 6(C). The investigation results that R(ω) has big peak at 0.28, indicating the absorption of photon in $EAGeCl_3$. The electron loss is presented in figure 6(D). The function describes the energy loss as high-speed electrons traverse from medium. The value of the loss function, L(ω), is approximately 0.1 in the region of visible light, suggesting limited attenuation in the $EAGeCl_3$ material.

3.4. Thermoelectric properties

Thermoelectric properties are important in enhancing the efficiency and device performance in the field of photovoltaics. ZT refers to a quantity without any dimension often used in the context of thermoelectric materials to quantify their efficiency has a strong relationship with the thermoelectric response of a material to a temperature difference and ability to generate an electric voltage, ability to conduct an electrical current, and ability to conduct heat. By considering these factors, researchers can identify and develop thermoelectric materials that are well-suited for their intended applications. These properties have been evaluated by BoltzTrap code it is likely a computational tool or software used for calculating electronic transport properties in materials based on the Boltzmann transport equation [45]. The graph between the temperature and chemical potential (μ) is demonstrated in figure 7-8. For an ideal thermoelectric material this ZT parameter $\left(ZT = \frac{S^2\sigma T}{\kappa}\right)$should approach to unity (1). One can achieve this result only when the material exhibits a balance between the ability of material to conduct electricity effectively and resist the flow of heat. Charge carriers with lower mass (such as electrons) are more mobile within the material, meaning they can move more freely in response to an electric field contribute to the higher electrical conductivity in the material. Conversely, charge carriers with higher mass (such as holes) tend to have higher value to generate electrical voltage or potential in response to temperature. They can enhance the figure of merit of a material with high Seebeck coefficient value, which is desirable for efficient thermoelectric performance. ZT for the material is approaches 1 when the chemical potential, which represents the energy level where there is an equal probability of adding and removing an electron, falls within the energy range where no electronic states are allowed, as depicted in figure 7 (A). This corresponds to the density of charge carriers within the material vary between 10^{18} and $10^{19}cm^3$. Figure 7(B) and 7(C) show the relationship between ZT and the concentrations of electrons and holes, respectively. Furthermore, these figures show that the ZT value is higher in $EAGeCl_3$ material, regardless of n-doped or p-doped. Nonetheless, when the doping concentration grows, these values gradually decrease. The ZT of n-type $EAGeCl_3$ material is sensitive to variations doping amount and temperature. Therefore, n-type $EAGeCl_3$ is a better candidate for thermoelectric applications compared to p-type $EAGeCl_3$.

A high Seebeck coefficient (S) ensures that the material can efficiently convert heat energy into electrical energy or vice versa, which is crucial for the effectiveness of thermoelectric devices. A negative S indicates that the material produces negative voltage when heated at one end, relative to the cooler end when the dominant charge carriers in the material are electrons and a positive S means that the material produces a positive voltage when heated at one end, relative to the cooler end when the dominant charge carriers are holes. Figure 7(D) demonstrates that Seebeck coefficient is significant when the chemical potential falls within the band gap of the material. It reaches a maximum value of -2.97mV/K at μ=0.64eV and 2.75mV/K at μ=-0.5eV at 300K. Figure 7(E) represents the plot of S *Vs* electron concentration (n), whereas Fig. 7(F) depicts the plot of S Vs hole concentration (n). These graphs show that the S drops as the concentration of electrons and holes increases while the temperature remains constant. However, either electron and hole doping is applied to the material the value of S increases as the temperature rises. In addition, when both electron and hole doping are at equivalent levels in the material at constant temperature the material with n-type doping (where the majority charge carriers are electrons) has higher S

value compared to the p-type material (where the majority charge carriers are holes). Furthermore, when the same level of electron and hole doping is present at the same temperature, the n-type material exhibits higher S value.

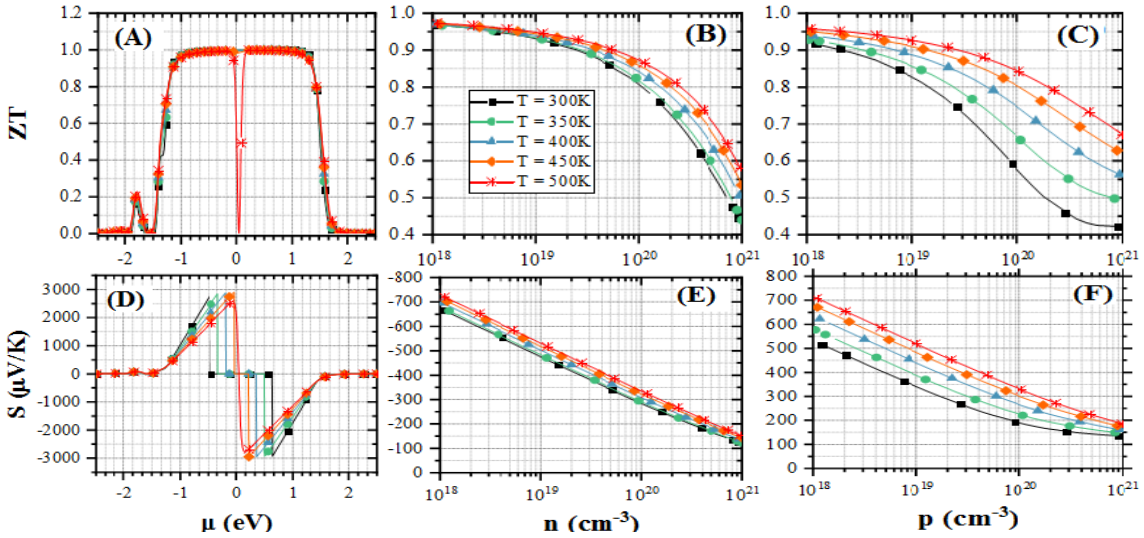

Fig. 7. (a) Figure of merit as a function of chemical potential, (b) Figure of merit as function of hole concentration, (c) Figure of merit as a function of electron concentration, (d) Seebeck coefficient as a function of chemical potential, (e) Seebeck coefficient as a function of hole concentration, (f) Seeback coefficient as a function of electron concentration.

The relationship of the electrical conductivity to the relaxation time (σ/τ) is framed as a function of chemical potential in figure 8(A). In figure 8(B) and 8(C) σ/τ is graphed as a function of electron concentration and hole concentration, respectively.

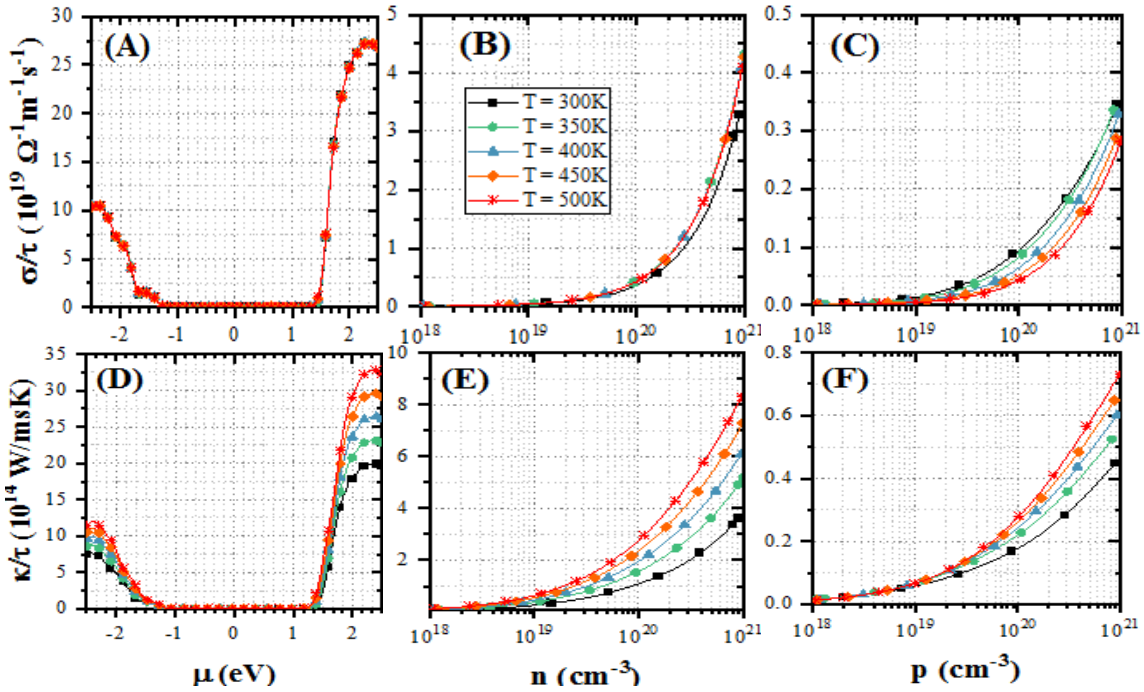

Fig. 8. (a) σ/τ as a function of chemicalpotential, (b) σ/τ as function of hole concentration, (c) σ/τ as a function of electron concentration, (d) κ/τ as a function of chemicalpotential, (e) κ/τ as a function of hole concentration, (f)) κ/τ as a function of electron concentration.

The ratio σ/τ reduces as the temperature rises in the p-type material. On the other hand in n-type materials, the ratio is not affected by the temperature. This suggests that electron mobility is not much affected by the variation in the temperature in $EAGeCl_3$. Figure 8(D), (E), and (F) show the ratio of thermal conductivity to relaxation time (κ/τ). This ratio is higher for the p type material at a particular doping level and temperature. This also shows that phonon scattering is higher in the n type material in comparison to the p type material. To prevent photovoltaic material from overheating the effective electrical conductivity should be high. Conversely the thermal conductivity should be low to protect and minimize the material from thermal loss. So according to the above discussion, one can see that the n-type $EAGeCl_3$ is the preferred photovoltaic material.

3.5. Thermal properties

Gibbs2 simulation code is used for the simulation of thermodynamic properties of $EAGeCl_3$ material in the 100-800K temperature range and 0-3GPa pressure range [45-49] using the quasi-harmonic Debye model. The Debye temperature varies linearly with the degree of interatomic bonding. The stronger the cohesive forces, the more they obstruct the motion of the atoms and prevent a crystal from compressing. Substances with high Debye temperatures eventually resist crystal compression. Figure 9(A) depicts the fluctuation in Debye temperature (θ_D) with temperature at 0-3GPa pressures. When the temperature rises, the Debye temperature also falls; yet, as pressure rises, the Debye temperature value rises. Entropy (S) measure the degree of disorder in a particular system. Figure 9(B) shows that the Entropy (S) is more temperature-dependent and less pressure-dependent. As the temperature rises, so does the value of S and at a particular temperature as the pressure increases the value of S decreases. Fig. 9(C) shows the effect of volume V (in $bohr^3$) on temperature at various pressures P (in GPa). The graph shows how the volume of a gas increases as its temperature rises at different pressures. Fig. 9(D) depicts the thermal expansion coefficient (α) concerning temperature and pressure variations. The value of α is sensitive between 0 and 200K, with a steady decrease in sensitivity above 200K.

The compound's bulk modulus was previously determined using a volume optimization method. The results obtained from the Gibbs algorithm, as depicted in Figure 9(E), supported these findings. It was noticed that the bulk modulus of $EAGeCl_3$ decreases with temperature increment at various pressures. The Grüneisen parameter is utilized (γ) to assess the degree of anharmonicity inside a crystal. As temperature rises, atomic movement becomes stronger, leading to heightened an-harmonic effects. The higher value of γ signifies increased photon scattering, resulting in diminished lattice thermal conductivity. Figure 9(F) demonstrated that γ steadily rises with rising temperature and at that time pressure is constant and γ decreases with increasing pressure under constant temperature, indicating reduced thermal conductivity for $EAGeCl_3$.

The compound's Bulk modulus was previously computed using Volume optimization. The results were obtained using the Gibbs algorithm, as shown in Fig 9(E), backed up these conclusions. The $EAGeCl_3$ Bulk modulus decreases as the temperature at various pressures rises. The Grüneisen parameter (γ) calculates the level of anharmonicity inside the material. The movements of atoms get stronger as the temperature rises, which results in enhanced anharmonic effects. A higher γ value tells about the high level of photon scattering; which results in a reduced lattice-thermal conductivity. Fig. 9(F) shows that, as expected, grows steadily with rising temperature at constant pressure and decreases with growing pressure under constant temperature. Hence, $EAGeCl_3$ has a reduced thermal conductivity.

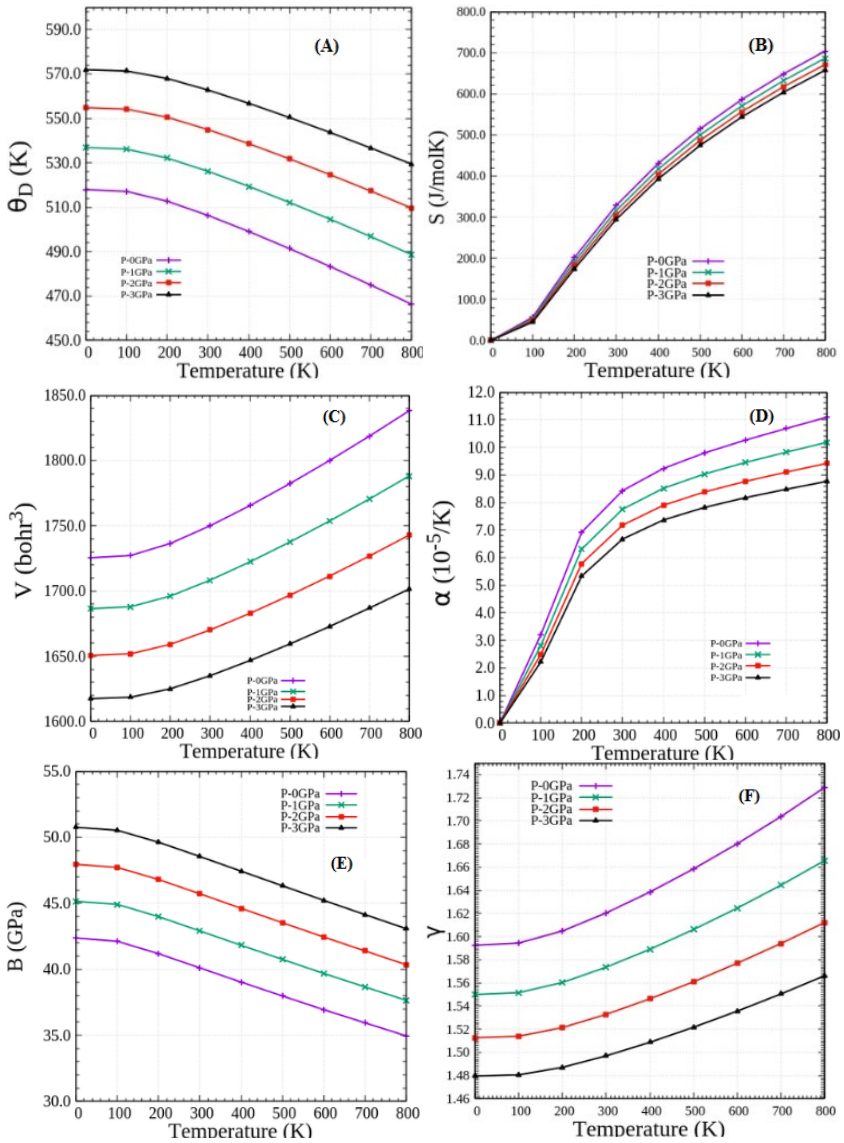

Fig. 9. (a) Debye temperature as a function of temperature at various pressures, (b) Entropy, (c) Volume, (d) Thermal expansion coefficient, (e) Bulk modulus and (f) Grüneisen parameter.

4. Conclusions

The material's structural, electrical and transport characteristics were examined using WIEN2K software. A comprehensive examination of its electrical and optical characteristics revealed it to be a direct band gap material with a value of 2.685 eV, demonstrating outstanding performance in both ultraviolet and visible spectrums. This confirms its significant potential for application in photovoltaic systems. Its thermodynamic stability allows it to achieve a ZT as unity at room temperature and 500K in both p and n type regions. This suggests that it could be used also in thermoelectric generators, providing efficient toxic-free energy across a wide temperature range. The investigation into this material's transport capabilities is groundbreaking, with hopes that these findings will establish an important foundation for future research in this field.

References

[1] A. Dubey, N. Pandit, R. Singh, T. K. Joshi, B. L. Choudhary, P. K. Kamlesh, S. Al-Qaisi, T. Kumar, K. Kaur, A. S. Verma, J. Molecular Modeling 30 (2024) 77; https://doi.org/10.1007/s00894-024-05867-7

[2] N. Pandit, A. Dubey, T. K. Joshi, A. Shukla, U. Rani, P. K. Kamlesh, R. Gupta, T. Kumar, K. Kaur, A. S. Verma, Inter. J. Modern Phy. B (2024) 2550059; https://doi.org/10.1142/S0217979225500596

[3] N. Pandit, R. Singh, A. Kumar, T. K. Joshi, A. Shukla, U. Rani, P. K. Kamlesh, T. Kumar, Priyanka, A. S. Verma, Modern Phy. Letters B (2024) 2450345; https://doi.org/10.1142/S0217984924503457

[4] J. Y. Kim, J. W. Lee, H. S. Jung, H. Shin, N. G. Park, Chemical Reviews 120 (2020) 7867-7918; https://doi.org/10.1021/acs.chemrev.0c00107

[5] U. Rani, P. K. Kamlesh, R. Agarwal., J. Kumari, A. S. Verma, Inter J. Quantum Chemistry 121 (2021) e26759; https://doi.org/10.1002/qua.26759

[6] P. K. Kamlesh, R. Gautam, S. Kumari, A. S. Verma, Physica B: Condensed Matter 615 (2021) 412536; https://doi.org/10.1016/j.physb.2020.412536

[7] Y. Soni, R. Agrawal., S. Pachori, A. Shukla, A. S. Verma, Physica Scripta 97 (2022) 055821; https://doi.org/10.1088/1402-4896/ac66a0

[8] S. Pachori, R. Agarwal., B. Prakash, S. Kumari, A. S. Verma, Energy Technology 10 (2022) 2100709; https://doi.org/10.1002/ente.202100709

[9] U. Rani, Y. Soni, P. K. Kamlesh, S. Pachori, A. S. Verma, Inter. J. Energy Research 45 (2021) 13442-13460; https://doi.org/10.1002/er.6673

[10] S. Choudhary, A. Shukla, J. Chaudhary, A. S. Verma, Inter J. Energy Research 44 (2020) 11614-11628; https://doi.org/10.1002/er.5786

[11] A. Shukla, V. K. Sharma, S. K. Gupta, A. S. Verma, Materials Chemistry and Physics 253 (2020) 123389; https://doi.org/10.1016/j.matchemphys.2020.123389

[12] J. Chaudhary, S. Choudhary, C. M. S. Negi, S. K. Gupta, A. S. Verma, Physica Scripta 94 (2019) 105821; https://doi.org/10.1088/1402-4896/ab2dc4

[13] W. Ke, M. G. Kanatzidis, Nature communications 10 (2019) 965; https://doi.org/10.1038/s41467-019-08918-3

[14] A. Krishna, S. Gottis, M. K. Nazeeruddin, F. Sauvage, Advanced Functional Materials 2 (2019) 1806482; https://doi.org/10.1002/adfm.201806482

[15] C. Motta, F. El-Mellouhi, S. Sanvito, Scientific Reports 5 (2015) 12746; https://doi.org/10.1038/srep12746

[16] Z. Zhang, D. Liu, K. Wu, Spectrochimica Acta Part A: Molecular and Biomolecular Spectroscopy 226 (2020) 117638; https://doi.org/10.1016/j.saa.2019.117638

[17] C. He, G. Zha, C. Deng, Y. An, R. Mao, Y. Liu, Z. Chen, Crystal Research and Technology 54 (2019) 1900011; https://doi.org/10.1002/crat.201900011

[18] F. Giustino, H. J. Snaith, ACS Energy Letters 1 (2016) 1233-1240; https://doi.org/10.1021/acsenergylett.6b00499

[19] S. Yang, W. Fu, Z. Zhang, H. Chen, C. Z. Li, J. Mater. Chem. A 5 (2017) 11462-11482; https://doi.org/10.1039/C7TA00366H

[20] G. Schileo, G. Grancini, J. Mater. Chem. C, 9 (2021) 67-76; https://doi.org/10.1039/D0TC04552G

[21] P. V. Kamat, J. Bisquert, J. Buriak, ACS Energy Letters 2 (2017) 904-905; https://doi.org/10.1021/acsenergylett.7b00246

[22] A. Babayigit, A. Ethirajan, M. Muller, B. Conings, Nature Materials 15 (2016) 247-251; https://doi.org/10.1038/nmat4572

[23] D. Liu, Q. Li, K. Wu, RSC advances 9 (2019) 7356-7361; https://doi.org/10.1039/C9RA00853E

[24] Y. Zhang, N. G. Park, J. Mater. Chem. A 8 (2020) 17420-17428; https://doi.org/10.1039/D0TA05799A
[25] T. K. Joshi, A. Shukla, G. Sharma, A. S. Verma, Inter J. Energy Research 45 (2021) 908-919; https://doi.org/10.1002/er.5985
[26] T. K. Joshi, Pravesh, G. Sharma, A. S. Verma Mater Sci Semicond Process 115 (2020) 105111; https://doi.org/10.1016/j.mssp.2020.105111
[27] F. Arkan, M. Izadyar, Computational Materials Science 152 (2018) 324-330; https://doi.org/10.1016/j.commatsci.2018.06.006
[28] T. K. Joshi, A. Shukla, G. Sharma, A. S. Verma, Materials Chemistry and Physics 251 (2020) 123103; https://doi.org/10.1016/j.matchemphys.2020.123103
[29] A. Mahmood, J.L. Wang, Energy Environ. Sci. 14 (2021) 90-105; https://doi.org/10.1039/D0EE02838J
[30] K. Schwarz, P. Blaha, S. B. Trickey, Mol. Phys. 108 (2010) 3147-3166; https://doi.org/10.1080/00268976.2010.506451
[31] J. P. Perdew, Y. Wang, Phys. Rev. B 45 (1992) 13244; https://doi.org/10.1103/PhysRevB.45.13244
[32] J. P. Perdew, K. Burke, M. Ernzerhof, Phys. Rev. Lett. 77 (1996) 3865; https://doi.org/10.1103/PhysRevLett.77.3865
[33] D. Koller, P. Blaha, F. Tran, J. Phys. Condens. Matter 25 (2013) 435503; https://doi.org/10.1088/0953-8984/25/43/435503
[34] M. Shishkin, G. Kresse, Phys. Rev. B 75 (2007) 235102; https://doi.org/10.1103/PhysRevB.75.235102
[35] D. Koller, F. Tran, P. Blaha, Phys. Rev. B 85 (2012) 1-8; https://doi.org/10.1103/PhysRevB.85.155109
[36] K. Ephraim Babu, N. Mural.i, K. VijayaBabu, P. T. Shibeshi, V. Veeraiah, Acta Phys. Pol. 125 (2014) 1179-1185; https://doi.org/10.12693/APhysPolA.125.1179
[37] J.P. Perdew, A. Ruzsinszky, G.I. Csonka, O.A. Vydrov, G.E. Scuseria, L.A. Constantin, K. Burke, Phys. Rev. Lett. 100 (2008) 136406; https://doi.org/10.1103/PhysRevLett.100.136406
[38] M. Derras, N. Hamdad, M. Derras, A. Gessoum, Results Phys. 3 (2013) 219-230; https://doi.org/10.1016/j.rinp.2013.09.011
[39] P. Hohenberg, W. Kohn, Physical review 136 (1964) B 864; https://doi.org/10.1103/PhysRev.136.B864
[40] A. D. Becke, M. R. Roussel, Physical Review 39 (1989) 3761; https://doi.org/10.1103/PhysRevA.39.3761
[41] F. D. Murnaghan, Proceedings of the National Academy of Sciences 30 (1944) 244-247; https://doi.org/10.1073/pnas.30.9.244
[42] F. D. Murnaghan, Proceedings of the National Academy of Sciences 30 (1944) 382-384; https://doi.org/10.1073/pnas.30.12.382
[43] A. Kumari, A. Nag, J. Kumar, Physics and Chemistry of Solids 161 (2022) 110430; https://doi.org/10.1016/j.jpcs.2021.110430
[44] Q. Mahmood, G. M. Mustafa, N. A. Kattan, T. Al.shahrani, N. Sfina, A. Mera, Z. H. Shah, H. H. Somaily, S. Al. harthi, M. A. Amin, Materials Science and Engineering: B 286 (2022) 116088; https://doi.org/10.1016/j.mseb.2022.116088
[45] G. K. Madsen, D. J. Singh, Computer Physics Communications 175 (2006) 67-71; https://doi.org/10.1016/j.cpc.2006.03.007
[46] E. Francisco, M. A. Blanco, G. Sanjurjo, Physical Review B 63(2001) 094107; https://doi.org/10.1103/PhysRevB.63.094107
[47] M. A. Blanco, A. M. Pendás, E. Francisco, J. M. Recio, R. Franco, Journal of Molecular Structure: THEOCHEM 368 (1996) 245-255; https://doi.org/10.1016/S0166-1280(96)90571-0
[48] R. Hill, Proceedings of the Physical Society. Section A 65 (1952) 349; https://doi.org/10.1088/0370-1298/65/5/307

[49] M. A. Blanco, E. Francisco, V. Luana, Computer Physics Communications 158 (2004) 57-72; https://doi.org/10.1016/j.comphy.2003.12.001